

# Assisted conduction in molecular wire and related quantum biological processes

Simon Pigeon,<sup>1,2</sup> Lorenzo Fusco,<sup>2</sup> Gabriele De Chiara,<sup>2</sup> and Mauro Paternostro<sup>2</sup>

<sup>1</sup>*Laboratoire Kastler Brossel, UPMC-Sorbonne Universités,  
CNRS, ENS-PSL Research University, Collège de France,  
4 place Jussieu Case 74, F-75005 Paris, France.*

<sup>2</sup>*Centre for Theoretical Atomic, Molecular and Optical Physics,  
School of Mathematics and Physics, Queen's University Belfast, Belfast BT7 1NN, United Kingdom*

We present a detailed study of the conduction properties of a molecular wire where hopping process between electronic sites is coupled to a molecular vibrational mode. The molecule is sandwiched between two electronic leads at finite temperatures. We show that the electro-mechanical coupling leads, in some cases, to a strong enhancement of the conduction from one lead to another. Moreover, the device can act as a transistor with proper driving of the molecular vibrational mode, passing sharply from enhanced conduction to short-circuit configuration. We also relate the system behavior to quantum biological phenomena such as light-energy harvesting and olfaction to show how the original microscopic model considered here can be a good candidate to describe those phenomena.

Molecular electronics was initially dedicated to the study of transport properties of molecule sandwiched between electronic leads. It was originally thought as an alternative platform to silicon electronics but it has matured lately as a rich and promising field of research beyond its initial scope [1, 2]. Numerous theoretical works have been dedicated to enlighten the behavior of such metal-molecule-metal junction depending on the microscopic description of the molecule. Most of them have focused on a description including solely connected electronic sites for building devices such as current rectifiers [3] or thermal transistors [4] for example. Rich features were predicted such as stochastic pumps [5, 6] or laser-induced phase-controllable transport [7] to mention only some recent results. Based on the rich nature of the molecule under study, more recently an additional ingredient was added to the microscopic description of these devices: the coupling of the conduction properties to the vibrational degrees of freedom of the molecule which is expected to play a crucial role on the transport properties of these systems [8, 9]. This configuration was first considered in order to cool (through side-band cooling) the mechanical/vibrational degree of freedom of the molecule [10, 11]. The study of the impact of this coupling on transport was also considered showing negative differential conductance [12–15] or other vibration-assisted transport phenomena [16–20]. However, this extended literature on the subject is only, to our knowledge, based on Anderson-Holstein-like models.

The Anderson-Holstein model consists of electronic sites sandwiched between two electronic leads while the vibrational mode is coupled to an electronic eigenstate, raising or lowering its energy depending on the vibrational state [21]. In this paper we present a similar setup, in which the molecular vibration is not coupled to an electronic eigenstate but to the hopping process taking place between two microscopic electronic sites. Consequently, as it will be detailed, controlling the vibration properties of the molecule we can tune the flux of electrons get through the system. This allows not only for an enhancement of the conduction, even when

no voltage bias is applied between the electronic leads, but also for a switching regime in which the current flowing is deterministically turned on and off. Moreover, we illustrate how the original microscopic model considered can be a very good candidate for recently proposed quantum biological processes.

The remainder of this paper is organized as follows: Sec. I introduces the system and the working conditions considered throughout our work. In Sec. IA, we adiabatically eliminate the vibrational degree of freedom to end up with an effective dynamics for the conducting part of the system. This analysis is then complemented by tracing out the leads degrees of freedom (Sec. IB). Sec. II is dedicated to the dynamics and related exchange statistics with the electronic leads. We detail the unraveling approach used to access the statistics of exchange taking place between the system and one of the electronic leads. We then pass to a systematic study of the mean current flowing through the device as a function of the electronic-lead configuration. For such a study, we focus on the low-temperature regime. We then switch to the study of more realistic conditions. We first illustrate the conduction enhancement together with demonstrating the transistor regime (Sec. III A) before to connect the observed phenomena to potential quantum biological processes such as light-energy harvesting and olfaction (Sec. III B). In Sec. IV we summarise our results and comment on other interesting features left unaddressed in our study.

## I. DESCRIPTION OF THE PHYSICAL SYSTEM

As illustrated in Fig. 1, the system being considered consists of two coupled parts: (i) an electronic wire and (ii) a vibrational mode. Here, we first focus on the Hamiltonian part of the dynamics of each subsystem and their coupling. Our model aims at capturing the salient features of the energy of a molecular wire. Such system consists of a three-modular molecular junction

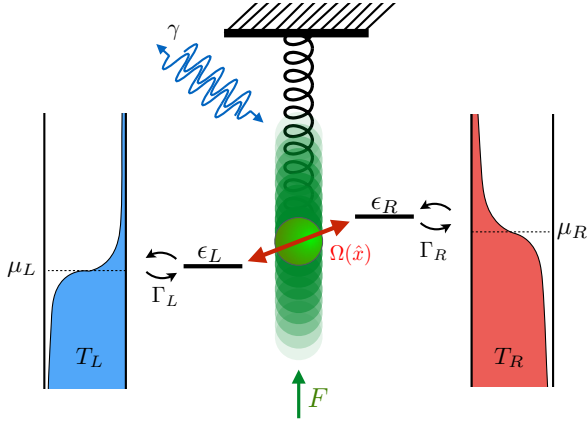


Figure 1. Schematics of the system representing the molecular wire connected to two electronic leads at given temperature  $T_R$  and  $T_L$ . The vibrational mode is represented by the harmonic oscillator in-between the two electronic sites and we define  $\Omega(\hat{x})$  the oscillator-controlled hopping between  $\epsilon_L$  and  $\epsilon_R$ .

encompassing a left ( $L$ ), right ( $R$ ) and central ( $C$ ) region. The  $L$  and  $R$  part of the junction are connected, through leads, to an external potential, thus putting the junction out of equilibrium and allowing for the circulation of an electronic current. The conductance of the junction depends on the conformation of the molecule itself: by putting part  $C$  out of the plane containing both  $L$  and  $R$  (which we assume to be coplanar), the resistance offered by the junction to the current can be varied in light of the modifications induced to the overlap of the electronic wave-functions that is responsible for the conduction. In what follows, we will focus on the case of small fluctuations around an otherwise stable molecular conformation (i.e. a stable relative angle between the central and peripheral parts of the molecular junction). The relative angle between the in-plane and out-of-plane parts of the junction would thus oscillate around the macroscopically stable configuration, such oscillations being treated quantum mechanically. A minimal model that is able to capture the essential conformational influences over electric conductance is as follows. We consider two single-occupation sites whose energy is given by the on-site Hamiltonian (where we have neglected the Coulomb interaction and have assumed units such that  $\hbar = 1$ )

$$\hat{H}_w = \epsilon_L \hat{s}_L^\dagger \hat{s}_L + \epsilon_R \hat{s}_R^\dagger \hat{s}_R. \quad (1)$$

Here,  $\hat{s}_{L/R}^{(\dagger)}$  is the annihilation (creation) operator of an electron occupying the left ( $L$ ) and right ( $R$ ) site. For simplicity we restrict ourselves to  $\epsilon_R - \epsilon_L = \Delta > 0$ . We have assumed that the electrons do not hop directly between sites, an assumption invoked only to simplify our approach but that does not affect the phenomenology that will be illustrated here. Our model also includes a vibrational mode, which is described under harmonic

approximation as

$$\hat{H}_v = \omega_v \left( \hat{a}^\dagger \hat{a} + \frac{1}{2} \right) + \sqrt{2} F \hat{x}. \quad (2)$$

Here,  $\omega_v$  is the vibrational frequency,  $\hat{a}^{(\dagger)}$  is the mode annihilation (creation) operator, and  $\hat{x} = (\hat{a} + \hat{a}^\dagger) / \sqrt{2}$  is the associated position-like operator. We consider the case of a harmonic oscillator driven by a constant force of strength  $F$ . Electronic and vibrational subsystems are coupled according to the model

$$\hat{H}_{w-v} = \Omega(\hat{x})(\hat{s}_R^\dagger \hat{s}_L + \hat{s}_L^\dagger \hat{s}_R), \quad (3)$$

which describes phonon-assisted inter-site hopping at a rate  $\Omega(\hat{x})$ , which in turn depends on the position of the oscillator, i.e. the molecular conformation. The total Hamiltonian of the system is thus

$$\hat{H} = \hat{H}_w + \hat{H}_{w-m} + \hat{H}_v. \quad (4)$$

The assumption of small oscillations around a stable configuration justifies a series expansion of the hopping rate as  $\Omega(\hat{x}) \approx \Omega_0 + \Omega_1 \hat{x}$ . This gives rise to a standard hopping mechanism connecting the two sites being considered, and a phonon-assisted one, occurring at rate  $\Omega_1$ , that depends explicitly on  $\hat{x}$ .

#### A. Vibrational mode damping and adiabatically eliminated model

Thermal excitations are a possible physical mechanism responsible for the oscillations around the stable molecular conformation. We thus consider a thermal reservoir coupled to the vibrational mode. This leads to the dynamical model

$$\partial_t \hat{\rho}_m = -i[\hat{H}_v, \hat{\rho}_m] + \mathcal{L}_v[\hat{\rho}_m], \quad (5)$$

where  $\hat{\rho}_m$  is the density matrix of the system and we have introduced the Lindblad dissipator

$$\mathcal{L}_v[\bullet] = \frac{\gamma \bar{n}}{2} D[\hat{a}^\dagger, \bullet] + \frac{\gamma(\bar{n} + 1)}{2} D[\hat{a}, \bullet], \quad (6)$$

where  $\gamma$  is the coupling strength to the bosonic bath,  $\bar{n}$  is the mean number of excitations in the bath (related to the bath's temperature by  $\bar{n} = 1/(\exp[\hbar\omega_v/k_B T_v] - 1)$ ), and  $D[\hat{O}, \bullet] = (2\hat{O} \bullet \hat{O}^\dagger - \{\hat{O}^\dagger \hat{O}, \bullet\})$ . The equation of motion of the annihilation operator of the vibrational mode reads

$$\partial_t \hat{a} = -i\omega_v \hat{a} - i\frac{\Omega_1}{\sqrt{2}} (\hat{s}_L^\dagger \hat{s}_R + \hat{s}_R^\dagger \hat{s}_L) - \frac{\gamma}{2} \hat{a} + F. \quad (7)$$

We assume that the oscillatory mode reaches its steady-state in a time much shorter than the characteristic time of the evolution of the system, so that we can advocate for the validity of the adiabatic approximation, according to which the state of the oscillator can be assumed to

be stationary and unaffected by the coupling to the electronic wire. Its degrees of freedom can thus be traced out to seek for an effective reduced dynamics of the electronic system. From Eq. (7), the steady-state position of the oscillator is

$$\hat{x}_{st} = -\frac{\Omega_1 \omega_v}{\omega_v^2 + \gamma^2/4} \left( \hat{s}_L^\dagger \hat{s}_R + \hat{s}_R^\dagger \hat{s}_L + F \right). \quad (8)$$

The Heisenberg evolution of the wire operator is

$$\partial_t \hat{s}_X = -i\epsilon_X \hat{s}_X + i(\Omega_0 + \Omega_1 \hat{x}) \hat{s}_Y \hat{s}_X^Z, \quad (9)$$

where  $\hat{s}_X^Z = [\hat{s}_X, \hat{s}_X^\dagger]$  and with  $X$  and  $Y$  are either  $R$  or  $L$ . Replacing  $\hat{x}$  with its steady-state solution  $\hat{x}_{st}$  in Eq. (8), we have

$$\partial_t \hat{s}_X \simeq -i\epsilon_X \hat{s}_X + i\Omega \hat{s}_Y \hat{s}_X^Z - i\delta \hat{s}_Y^Z \hat{s}_X, \quad (10)$$

where  $\delta = \Omega_1^2 \omega_v / (\omega_v^2 + \gamma^2/4) / 2\sqrt{2}$  and  $\Omega = \Omega_0 - \frac{\omega_v \sqrt{2}}{\omega_v^2 + \gamma^2/4} \Omega_1 F$ . Eq. (10) can be interpreted as the Heisenberg equation for the operator  $\hat{s}_X$  evolving according to the effective Hamiltonian

$$\hat{H}_{\text{eff}} = \epsilon_L \hat{s}_L^\dagger \hat{s}_L + \epsilon_R \hat{s}_R^\dagger \hat{s}_R + \Omega (\hat{s}_R^\dagger \hat{s}_L + \hat{s}_L^\dagger \hat{s}_R) - \delta \hat{s}_R^Z \hat{s}_L^Z, \quad (11)$$

which does not contain the oscillator's degrees of freedom.

The adiabatic elimination induces a significant change of the coherent part of the dynamics of the electronic subsystem, but also of the incoherent part. Indeed, the reduced electronic density matrix  $\hat{\rho} = \text{Tr}_v [\hat{\rho}_m]$  evolves according to the master equation

$$\partial_t \hat{\rho} = -i[\hat{H}_{\text{eff}}, \hat{\rho}] + \mathcal{L}_{\text{eff}}[\hat{\rho}] \quad (12)$$

with  $\mathcal{L}_{\text{eff}}$  that describes the effective dissipation induced by the vibrational mode on the wire subsystem

$$\mathcal{L}_{\text{eff}}[\bullet] = \Gamma_v [\hat{s}_L^\dagger \hat{s}_R \bullet \hat{s}_L^\dagger \hat{s}_R + D [\hat{s}_L^\dagger \hat{s}_R, \rho] + L \leftrightarrow R], \quad (13)$$

with  $\Gamma_v = \gamma\delta(2\bar{n} + 1)$ . This incoherent part of the wire subsystem dynamics encompasses two processes. The first one, corresponding to the first term in Eq. (13) (and the analogous one where label  $L$  is swapped with  $R$ ), randomly swaps the coherence between single occupancy states, while the second term (and analogous with  $L \leftrightarrow R$ ) allows for the incoherent hopping between both sites. It is worth noticing that this last process leads to an enhancement of the conduction through the wire. Moreover the strength of such an incoherent process depends directly on the temperature of the bath attached to the vibrational mode through the mean occupation number  $\bar{n}$ . Such decoherence induced by the molecular vibration conserves the number of excitations, stating that, under the assumptions considered here, there is no energy exchange between the wire and the vibronic system.

## B. Coupling to electronic leads

We find it convenient, for the continuation of our analysis, to move to the eigenbasis of the effective Hamiltonian in Eq. (11), which involves non-local states [24, 25], so as to get the diagonal operator

$$\hat{H}_{\text{eff}} = \sum_{X=0}^3 \epsilon_X \hat{c}_X^\dagger \hat{c}_X, \quad (14)$$

where  $\epsilon_X = -\delta, (\epsilon_L + \epsilon_R + 2\delta \mp \sqrt{\Delta^2 + 4\Omega^2})/2, \epsilon_L + \epsilon_R - \delta$  are the system energies (ordered so that  $\epsilon_0 < \epsilon_1 < \epsilon_2 < \epsilon_3$ ), corresponding to the non-local states  $|X\rangle$ . In what follows, we use a notation such that the states  $|AB\rangle$  ( $A, B \in \{0, 1\}$ ) represents configurations with  $A$  and  $B$  electrons in the left and right site, respectively. We call these *local-basis* states.

A close analysis reveals that the first and last eigenstates in the non-local basis are identical to those of the local one, that is  $\hat{c}_0^\dagger \hat{c}_0 = |0\rangle\langle 0| = |00\rangle\langle 00|$  where no electrons are in the system and  $\hat{c}_3^\dagger \hat{c}_3 = |3\rangle\langle 3| = |11\rangle\langle 11|$  where one electron is on each sites. Notice that the Hamiltonian in Eq. (11) does not couple subspaces with a different total number of electrons in the sites. The intermediate states  $|01\rangle$  and  $|10\rangle$  are instead coupled to give rise to the non-local states  $|1, 2\rangle$  as

$$\begin{pmatrix} |1\rangle \\ |2\rangle \end{pmatrix} = U^{-1} \begin{pmatrix} |01\rangle \\ |10\rangle \end{pmatrix} \quad (15)$$

with  $U$  the change-of-basis matrix

$$U = \frac{2\Omega}{1-\alpha} \begin{pmatrix} 1-\alpha & 1+\alpha \\ \beta & -\beta \end{pmatrix}, \quad (16)$$

where we have introduced the parameters  $\alpha = \Delta/\sqrt{\Delta^2 + 4\Omega^2}$  and  $\beta = 2\Omega/\sqrt{\Delta^2 + 4\Omega^2}$ .

Let us now connect each electronic site to a lead. The picture we have in mind can be sketched as in Fig. 1, where each electronic site is individually coupled to its own fermionic bath. The Hamiltonian of each lead is

$$\hat{H}_\nu = \sum_i \epsilon_i^\nu \hat{c}_{\nu i}^\dagger \hat{c}_{\nu i}, \quad (17)$$

where  $\nu \in \{L, R\}$  refers to the left or right lead and  $\hat{c}_{\nu i}$  ( $\hat{c}_{\nu i}^\dagger$ ) the fermionic destruction (creation) operator for the  $i^{\text{th}}$  mode in the  $\nu$  bath. The coupling between the electronic sites and each lead is of the hopping form

$$\hat{H}_{\nu\text{-w}} = \Gamma_\nu \sum_i (\hat{c}_{\nu i}^\dagger \hat{s}_\nu + \hat{c}_{\nu i} \hat{s}_\nu^\dagger). \quad (18)$$

We will now eliminate the leads' degrees of freedom. Writing Eq. (18) in the eigenbasis of the electronic subsystem, we have

$$\begin{aligned} \hat{H}_{\nu\text{-w}} = & \frac{\Gamma_\nu}{2} \sum_{a=1}^2 \sum_i \left[ T_{2,a}^\nu \left( \hat{c}_{\nu i}^\dagger \hat{c}_a + \hat{c}_{\nu i} \hat{c}_a^\dagger \right) \right. \\ & \left. + T_{1,a}^\nu \left( \hat{c}_{\nu i}^\dagger \hat{c}_3^\dagger \hat{c}_a + \hat{c}_{\nu i} \hat{c}_a^\dagger \hat{c}_3 \right) \right] \end{aligned} \quad (19)$$

with  $\mathbf{T}^R = U$  and  $\mathbf{T}^L = \begin{pmatrix} 0 & 1 \\ 1 & 0 \end{pmatrix} U$ . The first (second)

line of Eq. (19) describes the transition between the wire ground state  $|0\rangle$  (highest energy state  $|3\rangle$ ) and an intermediate state (either  $|1\rangle$  or  $|2\rangle$ ). As in Refs. [24, 25], assuming the Born-Markov approximation, we eliminate the degrees of freedoms of both leads, giving rise to two effective dissipators  $\hat{\mathcal{L}}^\nu$ , i.e. one per lead, as defined in Appendix IV. For simplicity we assume the leads to act as two similar Ohmic baths with Fermi distribution at chemical potential  $\mu_\nu$  given by

$$f_\nu(\epsilon) = \frac{1}{e^{(\mu_\nu - \epsilon)/k_B T_\nu} + 1} \quad (\nu = L, R). \quad (20)$$

The number of excitations in the leads is taken to be the same (that is  $n_L(\epsilon) = n_R(\epsilon) = n$ ) and we choose the coupling strength  $\Gamma^L = \Gamma^R = \Gamma/n\pi$ . In this way, the only difference between the two leads consists in the respective chemical potentials  $\mu_R \neq \mu_L$ . We decompose the dissipation due to the leads, taken in the local picture as  $\hat{\mathcal{L}} = \hat{\mathcal{L}}_A + \hat{\mathcal{L}}_C$ , where the first refers to usual amplitude damping channel and the second one to decoherence. Both are explicitly defined in Appendix IV [Eq. (31) and (36) respectively]. Notice that last term  $\hat{\mathcal{L}}_C$  is not of a dephasing type because it changes the system energy as well as coherences.

Despite a rather simple system the dynamics taking place and especially the dissipation acting on the system is rich. We will now focus on this dynamics in order to determine the exchange taking place between the system and the leads.

## II. WIRE DYNAMICS AND EXCHANGE STATISTICS

In this Section we discuss the evolution of the electronic subsystem driven by its effective dynamics and connect it to the exchange statistics with the leads, using the thermodynamics of trajectories (Sec. II A). We then develop a systematic approach to identify the regime maximizing the enhancement effect provided to the current crossing the devices (Sec. II B) arising from the presence of the vibrational mode.

### A. Evolution of the electronic system and exchange statistics

In order to find the stationary state of the system we restrict ourselves to the evolution of the diagonal elements of the density matrix  $\hat{\rho}$  in the local basis. However, due to the interaction and possible hybridization of intermediate levels, terms such as  $|10\rangle\langle 01|$  and  $|01\rangle\langle 10|$  are also crucial. The dynamics of the electronic system can be tracked by writing its density matrix in vector form as  $\boldsymbol{\rho} = (\langle 00|\hat{\rho}|00\rangle, \langle 01|\hat{\rho}|01\rangle, \langle 10|\hat{\rho}|10\rangle, \langle 11|\hat{\rho}|11\rangle,$

$\langle 01|\hat{\rho}|10\rangle, \langle 10|\hat{\rho}|01\rangle)^T$ , and the master equation as

$$\partial_t \boldsymbol{\rho} = \mathcal{W} \boldsymbol{\rho}. \quad (21)$$

The form of the superoperator  $\mathcal{W}$ , which is not essential for the discussions to follow, is provided in Appendix IV. The resulting dynamics is similar to the one found in Ref. [25], albeit with specific features that should be stressed. Among them, the most significant is that the incoherent hopping induced by the vibrational mode acts directly on both the coherences ( $\langle 01|\hat{\rho}|10\rangle$  and  $\langle 10|\hat{\rho}|01\rangle$ ) of the electronic density matrix, and the occupations of the intermediate states ( $\langle 01|\hat{\rho}|01\rangle$  and  $\langle 10|\hat{\rho}|10\rangle$ ).

To determine the exchange statistics taking place between the system and the leads we now use the formalism of thermodynamics of trajectories [26–28]: We define a counting process of the net exchange of excitations between the system and the right leads such as  $K := \sum_{a=1}^2 \sum_{b=\{0,3\}} K_{a \leftrightarrow b}^R - J_{a \leftrightarrow b}^R$ , where  $K_{a \leftrightarrow b}^\nu$  ( $J_{a \leftrightarrow b}^\nu$ ) refers to an increment related to excitations leaving (entering) the system to (from) the lead  $\nu$  inducing a transition between level  $a$  and  $b$ . The introduction of such process modifies the dynamics of the electronic density matrix, which now obeys the biased master equation  $\partial_t \hat{\rho}_s = \mathcal{W}[\hat{\rho}_s] + \mathcal{L}_s[\hat{\rho}_s]$  where the biasing contribution to the evolution  $\hat{\mathcal{L}}_s$  is defined in Eq. (39) and where  $\hat{\rho}_s = \sum_K e^{-sK} P^K \hat{\rho}$  is the biased density matrix with  $P^K$  a projector over the subspace where the selected counting process results in  $K$  excitations being exchanged. As done previously, we consider the evolution of the vector of relevant density matrix elements  $\boldsymbol{\rho}_s = (\langle 00|\hat{\rho}_s|00\rangle, \langle 01|\hat{\rho}_s|01\rangle, \langle 10|\hat{\rho}_s|10\rangle, \langle 11|\hat{\rho}_s|11\rangle, \langle 01|\hat{\rho}_s|10\rangle, \langle 10|\hat{\rho}_s|01\rangle)^T$ , which occurs as  $\partial_t \boldsymbol{\rho}_s = (\mathcal{W} + \mathcal{L}_s) \boldsymbol{\rho}_s$ , where  $\mathcal{L}_s$  is given in Appendix IV.

The interesting feature of this system is that even the evolution of the coherences may induce changes on the counting statistics. At this stage, we can formally access the large deviation function  $\theta(s)$  (scaled cumulant generating function) encoding the full counting statistics defined as

$$\theta(s) = \lim_{t \rightarrow \infty} \frac{1}{t} \ln \left( \mathbf{x}^T \hat{T} [e^{\mathcal{W}_s t}] \boldsymbol{\rho}_s(0) \right), \quad (22)$$

where  $\mathcal{W}_s = \mathcal{W} + \mathcal{L}_s$ ,  $\mathbf{x} = (1, 1, 1, 1, 0, 0)^T$  and  $\hat{T}$  the time ordering operator. Through the diagonalization of the propagator  $\mathcal{W}_s$  one can access directly  $\theta(s)$ . The latter is aptly determined as the eigenvalue of  $\mathcal{W}_s$  with the longest decay time. More directly we can access also the first cumulants of the chosen exchange statistics using a bypassing approach not requiring numerical coarse-graining, similar to the one introduced in Ref. [28]. We thus have, as the first cumulant (moment), the mean current flowing through the system

$$\kappa_1 = -\text{Tr} \{ \mathcal{L}'_0[\tilde{\rho}] \} = -\mathbf{x}^T \mathcal{L}'_0 \tilde{\rho} \quad (23)$$

with  $\tilde{\rho}$  the steady-state solution of the density matrix  $\rho(t)$  and  $\tilde{\rho}$  the steady-state solution of its vectorized version and with  $\mathcal{L}'_0 = \partial_s \mathcal{L}_s|_{s=0}$ .



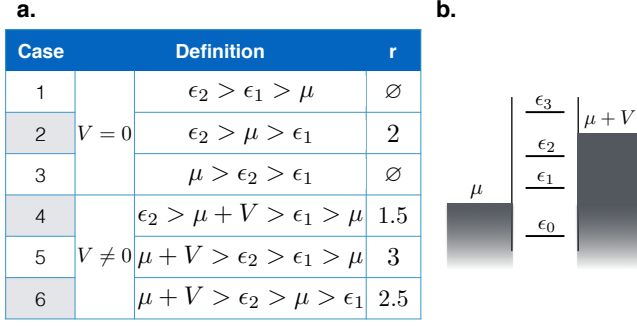


Figure 2. **a.** Table summarizing the six different cases considered in the body of the manuscript. We have defined  $\Omega = r\Delta$  with the value taken by  $r$  reported in the third column of the table. **b.** Illustration of the energy diagram corresponding to case 5.

The second cumulant is related to the variance of the current crossing the device, and can be determined as

$$\kappa_2 = \text{Tr} \{ \mathcal{L}_0''[\tilde{\rho}] + 2\mathcal{L}_0'[\tilde{\rho}'] \} = \mathbf{x}^T (\mathcal{L}_0''\tilde{\rho} + 2\mathcal{L}_0'\tilde{\rho}'), \quad (24)$$

where  $\tilde{\rho}' = \partial_s \tilde{\rho}_s|_{s=0}$  is the steady-state solution of the first order biased density matrix evolving according to

$$\partial_t \rho' = \mathcal{W}\rho' + (\mathcal{L}_0' - (\mathbf{x}^T \mathcal{L}_0' \rho) \mathbb{1}) \rho, \quad (25)$$

and where  $\mathbb{1}$  is the identity matrix. Notice that, by definition, we have  $\text{Tr} \{ \rho' \} = \mathbf{x}^T \rho' = 0$ .

According to this framework [28], after finding the steady state solution of the density matrix  $\tilde{\rho}$  we can access the mean current, while by solving  $\tilde{\rho}$  and  $\tilde{\rho}'$  we access the variance of the current flux.

## B. Systematic study of the different regimes

In order to understand the dynamics taking place we now assume that the incoherent hopping strength  $\Gamma_v$  is independent of the other parameters. The idea here is to find out which range of parameters gives rise to the largest enhancement due to the presence of the vibrational mode. In order to do so we distinguish between six different cases depending on the leads configuration, as summarized in the table reported in Fig. 2 **a.**, where we have set  $\Omega = r\Delta$ . For simplicity we consider here the case where the electronic leads are at zero temperature, leading to the following simplification

$$f_\nu(\epsilon) \xrightarrow{T_\nu \rightarrow 0} \Theta(\mu_\nu - \epsilon), \quad (26)$$

where  $\Theta(x)$  is the Heaviside function of argument  $x$ . In this condition we find that cases 1 and 3, with no bias voltage applied between the two leads and with their chemical potential respectively below  $\epsilon_1$  and above  $\epsilon_2$ , give a zero mean current. Conversely case 2, where  $\mu$  lies between  $\epsilon_1$  and  $\epsilon_2$ , corresponds to a non-zero net flux from  $L$  to  $R$ . This case is of special interest as

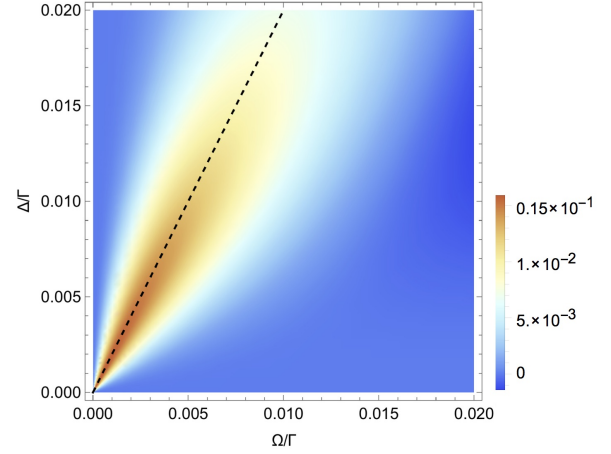


Figure 3. Enhancement induced by incoherent hopping. Difference  $\kappa_1 - \kappa_1^0$  (where  $\kappa_1^0$  is the net exchange neglecting incoherent hopping,  $\Gamma_v = 0$ ), describing the impact of the presence of the vibrational mode. In the vertical axis we have as a parameter the splitting between the energy level of each site  $\Delta = \epsilon_R - \epsilon_L$ , normalized by the coupling strength to the leads  $\Gamma$ . The horizontal axis corresponds to coupling strength  $\Omega$  between the two physical electronic sites, normalized by  $\Gamma$ . The black dashed line represents the maximum enhancement for given  $\Omega$  and  $\Delta$ . The parameter are such as  $\Gamma/\Gamma_v = 0.1$

it allows for conduction without need of bias voltage. This derives from the conformation of the system. In fact, such a net flux is also present without taking into account the molecular vibration. However, the presence of the vibrational mode gives rise to a significant enhancement on the conduction process, as shown in Fig. 3, where we present the difference between the net flux crossing the system with and without incoherent hopping as a function of  $\Delta$  and  $\Omega$ . As we can see, in case 2 the maximum enhancement occurs for  $\Omega = 2\Delta$ . Moreover, the enhancement gets more significant as  $\Omega$  and  $\Delta$  tend to zero. This comes from the fact that for  $\Omega \rightarrow 0$  we have clearly  $\kappa_1 \rightarrow 0$  if  $\Gamma_v = 0$ , while for  $\Gamma_v \neq 0$  and  $\Omega = r\Delta$ ,  $\kappa_1$  tends to be constant. Consequently, in this case, for small  $\Delta$  and  $\Omega$ , the conduction process is dominated by incoherent hopping induced by the vibrational mode. In this case we find that the relation  $\Omega = r\Delta$  gives rise to the smallest Fano factor ( $\kappa_2/\kappa_1$ ) depending on  $\Omega$  and  $\Delta$ , which is smaller than 1 and converging monotonously to 1 while increasing  $\Omega$  and  $\Delta$ , which indicates anti-bunching of the electron emission.

The remaining three cases all include a bias voltage (cf. Fig. 2). In all of them we have observed a similar conduction enhancement provided by the presence of the vibrational mode. The only difference with respect to Fig. 3 is the ratio between  $\Omega$  and  $\Delta$  associated to the maximal enhancement, which are as listed in Fig. 2 **a.** However, while the quantitative enhancement is very similar in all such cases, the qualitative behaviours are not necessary similar. For example, case 4 may present

reversed conduction flux in some region of the parameter space (for  $\Omega > r\Delta$ ). Cases 5 and 6, conversely, present always a positive current, whereas in case 2 an almost constant current is observed for  $\Omega = r\Delta$ . Considering the reduction of the Fano factor, its behaviour does not generally correspond to the maximal enhancement. Except for case 2, the smallest Fano factor does not coincide to  $\Omega = r\Delta$  with  $r$  as listed in Fig. 2. **a.** The smallest Fano factor was observed in both cases 5 and 6 for  $\Omega/\Delta = 4$ .

As the main objective of our investigation was the demonstration of conduction enhancement arising from the presence of the vibrational mode, we will not go deeper into the analysis of the six cases presented herein. Instead, we now focus on a more physical configuration where the interdependence of the parameter is fully taken into account.

### III. PHYSICAL IMPLICATION AND RELATED PHENOMENA

In this Section we will draw a less systematic but more practical picture of the situation under scrutiny to highlight the relevance of the effect induced by the vibrational mode on the electric conduction. Firstly, from a device perspective we will illustrate how the enhancement takes place under realistic conditions and how the control of the vibrational mode can lead to a control of the electronic flux. Next we will link the considered system to (i) high efficiency light-energy harvesting in molecular photosynthetic complexes and (ii) high-efficiency molecular identification in olfaction processes. Both these classes of processes are currently believed to benefit from quantum features [29].

#### A. Conduction enhancement and switching effect

Fig. 4 shows the mean current  $\langle I \rangle = \kappa_1$  passing through the wire as a function of the applied biased  $V$ , which is the most natural and accessible control parameter to adjust, and for different values of the incoherent hopping strength  $\Gamma_v$ . In the inset we represent the corresponding Fano factor. We notice the appearance of a plateau in the conduction in correspondence of the passage from one of the cases described in the previous Section to the next. The smoothing of the edges of those plateaux directly results from the finite temperature used for the electronic leads. Panel **a.** corresponds to a case where the coherent hopping strength  $\Omega$  between the left and right sites is one order of magnitude less than for the lower panel **b.**, while keeping the ratio  $\Delta/\Omega$  identical. From these two graphs we can clearly see that the enhancing effect is stronger as we decrease  $\Omega$  (and  $\Delta$ ). The picture regarding the Fano factor, on the other hand, is less straightforward. For high  $\Omega$ , the changes are relatively small and monotonic with respect to  $\Gamma_v$ . For smaller  $\Omega$  the changes induced

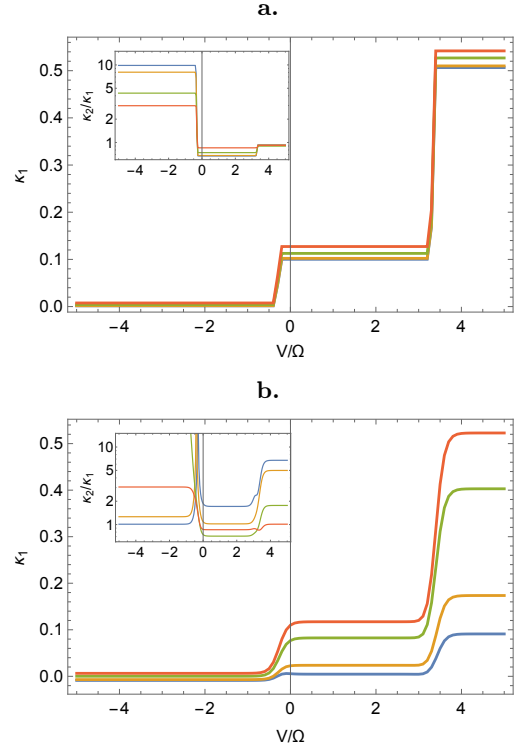


Figure 4. Net exchange as a function of the bias voltage  $V$  for  $\Delta/\Omega = 3$  for various values of the incoherent hopping strength  $\Gamma_v$  (respectively 0, 0.1, 1 and 10 for the blue, yellow, green and red curves). Inset represents corresponding Fano factor. Panel **a.** is for  $\Omega = 0.1$ , while panel **b.** is for  $\Omega = 1$ . Other parameters are such as  $k_B T_L = k_B T_R = 0.01$ ,  $\delta = \epsilon_L = \mu = 0$ , and  $\Gamma = 1$

by varying  $\Gamma_v$  are more complex. The spike observed close to  $V = 0$  for some line, corresponds to cases where the mean emission  $\kappa_1$  changes sign. Notice that the dependence on the bias voltage is normalized with respect to  $\Omega$  to focus on the enhancing effect provided by the vibrational mode. This renormalisation is at the origin of a more important smoothing effect of the edge due to the temperature. Notice also that at zero bias we have conduction taking place, and this conduction process is not intrinsic to the presence of the vibrational mode even if it is strongly enhanced by it.

However  $\Omega$  is, in principle, not easily accessible, in particular in light of its dependence on other relevant parameters of the system. Indeed, we have

$$\Omega = \Omega_0 - \frac{\omega_v \sqrt{2}}{\omega_v^2 + \gamma^2/4} \Omega_1 F, \quad (27)$$

where  $\omega_v$  is the oscillator frequency,  $\gamma$  its damping rate and  $F$  is the driving force (if any),  $\Omega_0$  is the bare hopping rate, independent of the molecular vibrational properties [0<sup>th</sup> order expansion of  $\Omega(\hat{x})$ ], while  $\Omega_1$  is the coupling strength between the oscillator position and the electronic hopping. It is worth reminding that, as shown previously, a key requirement to maximize the enhancement effect is to get the ratio  $\Delta/\Omega$  as in Fig. 2

a. with  $\Delta$  and  $\Omega$  as small as possible. Given Eq. (27), fine tuning of  $\Omega$  can be done through modulating the amplitude  $F$  of the driving force applied to the oscillator. The other parameter directly connected to the oscillator properties is the incoherent hopping strength

$$\Gamma_v = \frac{\gamma(\bar{n} + 1/2)\Omega_1^2\omega_v^2}{\sqrt{2}(\omega_v^2 + \gamma^2/4)^2}, \quad (28)$$

where  $\bar{n} = (\exp[\hbar\omega_v/k_B T_v] - 1)^{-1}$  corresponds to the density of excitation in the bosonic bath connected to the vibrational mode. From Eq. (28) we see that raising the temperature of the bath  $T_v$  leads to a direct increase of  $\Gamma_v$ . Consequently, by playing with a driving force  $F$  applied to the oscillator and the temperature of the corresponding bath  $T_v$ , one can independently manipulate both  $\Omega$  and  $\Gamma_v$ . Notice also that the energy level of the system depends on  $\delta = \frac{\Omega_1^2\omega_v}{2\sqrt{2}(\omega_v^2 + \gamma^2/4)}$ . This interdependence of the key parameters makes the previous systematic approach difficult to sustain in this context.

Nevertheless, Eq. (27) suggests that, for the amplitude  $F_{\text{crit}} = \Omega_0 (\omega_v^2 + \gamma^2/4) / (\sqrt{2}\omega_v\Omega_1)$  of the driving force, the effective Hamiltonian of the wire Eq. (11) leads to a short-circuit scenario where the two electronic sites become uncoupled, thus inhibiting the conduction through the wire. In Fig. 5 we plot the mean current through the device as a function of the voltage bias  $V$  and the driving force  $F$ . As  $V$  is varied, we clearly identify the two situations illustrated in the previous Section. More specifically: for  $F = 0$  we have a strongly conducting regime for high  $V$ . If, starting from this point in the parameter space, we increase slightly the applied driving force toward  $F_{\text{crit}}$ , we see a strong modification of the conduction, which leads to the short-circuit regime. Differently from the mechanism highlighted in Ref. [7], the switching on and off of the conduction does not require a complex driving of the electronic sites, although both our scheme and Ref. [7] allow for a non-zero conduction even if no voltage bias is applied between the electronic leads [cf. Fig. 5]. Consequently, beside allowing for an independent control of the key parameters  $\Gamma_v$  and  $\Omega$  (through the control of  $F$  and  $T_v$ , respectively), in our model the conduction can be switched on and off through a simple mechanical pressure on the molecule.

## B. Light-energy harvesting and olfaction

Here we discuss possible connections that the enhancement effect has with existing quantum descriptions of biological processes, and more specifically energy harvesting in photo-systemic molecular complex and olfaction [29]. To better mimic biological conditions we will consider only a situation where no voltage bias and driving force are applied. Even in such conditions, the interesting features observed previously are strong making this model a good candidate to explain these highly efficient biological processes.

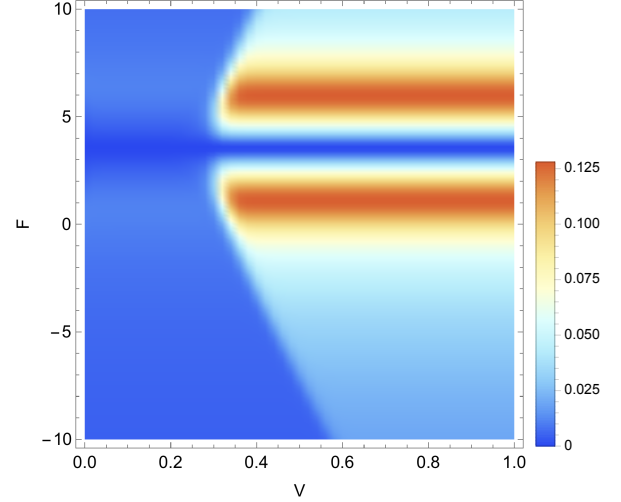


Figure 5. Mean current crossing the device ( $\kappa_1 = I$ ) as a function of the voltage bias  $V$  and the driving force  $F$ . The elected parameters are such as  $\mu = \epsilon_L = \Gamma = \gamma = 1$ ,  $\Omega_1 = 0.5$ ,  $T_L = T_R = T_v/100 = 0.01/k_B$ ,  $\Delta = 3\Omega_0 = 0.3$  and  $\omega_v = 0.01$ .

### 1. Light-energy harvesting and noise-assisted transport

Molecular complexes are highly efficient in the conduction of charge produced by photosynthesis [29, 30]. The general idea is that the transport across the molecular complex is in some way enhanced through interaction with vibrational modes of the molecule. Among the different phenomena which were considered to explain this high efficiency one strong candidate is known as noise-assisted transport [31–33]. This phenomenon, related to stochastic resonance [34], assumes that the fluctuations introduced in the electronic channel by the vibrational mode are responsible for enhanced conductivity. This corresponds exactly to what we reported in the previous Section. The higher  $\bar{n}$ , the bigger will be  $\Gamma_v$  the incoherent hopping strength and then lead to an enhanced conductivity. To illustrate such effect, in Fig. 6 we report the current through the device as a function of  $\Omega_1$ . The various lines refer to different vibrational and lead temperatures. As discussed previously, an increase of the vibrational mode's temperature, e.g. fluctuations of larger amplitudes, leads to an enhanced conduction. In order to maximize this effect, we need to fulfill the criteria detailed in Sec. II B ( $\Delta/\Omega \approx 2.5$  and  $\Delta$  small). The enhancement effect appears to be present in a wide range of values of  $\Omega_1$ , even weak ones. Notice that for large  $\Omega_1$  the adiabatic approach used above ceases to be justified. Finally, the difference between the full and dashed lines indicates that a further increase of the leads' temperature results in a drop of the conductivity of the wire. However, the enhancement effect appears to be robust against the leads temperature, making this model a very good candidate to explain light-energy harvesting in photosynthesis complex.

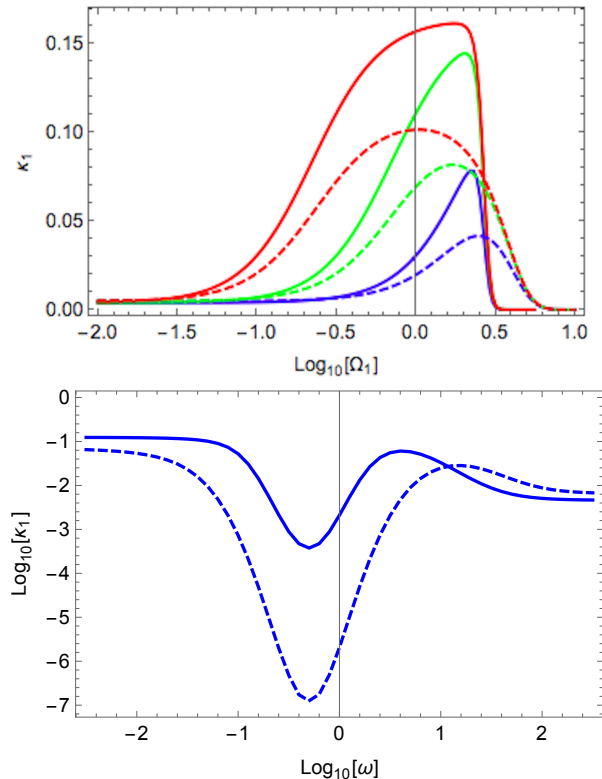


Figure 6. On the upper panel mean emission ( $\kappa_1$ ) as a function of the coupling strength to the oscillator  $\Omega_1$  (logarithmic scale) for different temperature. Full lines correspond to leads temperature  $T_R = T_L = 0.01$  while the dashed lines to warmer situation  $T_R = T_L = 0.1$ . The three colored lines, blue, green and red respectively correspond to a vibrational mode at equilibrium with a thermal bath at temperature  $T_v = 0.1, 1$  and  $10$  where  $\omega_v = 0.01$ . On the lower panel mean emission ( $\kappa_1$  in logarithm scale) as a function of the vibrational frequency  $\omega_v$  (logarithm scale). As previously the full line corresponds to leads at temperature  $T_L = T_R = 0.01$  and  $\Omega_1 = 0.5$ , while the dashed line to  $T_L = T_R = 0.1$  and  $\Omega_1 = 2$ . The other parameters are such as  $\mu = 0.9$ ,  $\Delta = 0.3$ ,  $\Omega_0 = 0.2$ ,  $\epsilon_L = \Gamma = \gamma = 1$  and  $V = F = 0$ .

Unlike other existing microscopic model presenting thermal-assisted transport, the effect here is strong and robust. This is because the fluctuation of the vibration mode ( $\bar{n}$ ) only affects the incoherent hopping  $\Gamma_v(\bar{n})$  and not the other key parameter. Neither  $\Omega$  nor the energy eigenstates of the system depend on it, which make highly feasible the observation of such effect in actual molecular electronic systems.

## 2. Olfaction and frequency analyze

The high efficiency of smell receptors has attracted attention, recently [35–37]. An accredited model of the way such receptors work consists of molecules taking physically place between two branches of the receptor. Each one of these branches acts as an electronic lead.

An electronic current would then have to go through or near the molecule. This proximity makes the current exchange strongly sensitive to the molecular properties, thus allowing for its characterization [36]. Such description [37] is very close to the model explored in this paper.

However, the microscopic coupling between electronic part and vibrational part in our system is rather different to the one considered in Ref. [37]. In the latter, an electron was assumed to pass physically through a molecule eigenstate carrying out necessary information to analyze the molecule, whereas in our case the molecule only affects the way the hopping processes take place. Moreover we do not need to assume any electronic bias between the two electronics leads.

In the lower panel of Fig. 6 we plot the mean current in logarithmic scale as a function of the mechanical mode frequency  $\omega_v$ . In the condition considered we see that the emission depends strongly on  $\omega_v$  varying of many order of magnitude. As every key parameter of the effective model depends on this frequency, tuning it in suitable ways leads to a strong dependence on the emission as pictured in the lower panel of Fig. 6. If for the given frequency the system is at the verge of one of cases previously detailed, changing  $\omega_v$  may change the system configuration therefore affecting dramatically the conductance. In the case considered the molecule acts as a band-stop filter which can be used to spectrally distinguish different molecules.

## IV. CONCLUSION

We have presented a detailed study of the conduction properties of a molecular wire coupled to a vibrational system via electronic hopping exchange. This description is inspired by the idea that physically the vibrational mode does not need to change the energetic structure of the electronic part but can just perturb the exchange taking place on this subsystem. We showed that the presence of the vibrational system can give rise to strong enhancement of the wire conductivity. Moreover through the control of the vibrational properties (temperature and position) one can accurately control the electronic flux crossing the device. An increase of the temperature enhances the conduction, while the control of the equilibrium position of the oscillator can switch on and off the conduction. We have suggested that the identified mechanism can be related to two biological quantum processes in light of the strong similarities between our model and mechanisms for noise-assisted transport. Such connections deserve more analysis, which is the objective of forthcoming studies.

## ACKNOWLEDGMENTS

We thank the EU FP7-funded Collaborative Project TherMiQ, the John Templeton Foundation (grant



number 43467), the Julian Schwinger Foundation (grant number JSF-14-7-0000), the UK EPSRC (grants

EP/M003019/1 and EP/P00282X/1) and the French ANR (ANR-16-ACHN-0027).

- 
- [1] S. V. Aradhya and L. Venkataraman, Single-molecule junctions beyond electronic transport. *Nat. Nanotechnol.* **8**, 399 (2013).
  - [2] L. Venkataraman, Klare, Nuckolls, Hybertsen, Steigerward, Dependence of single molecule junction conductance on molecular conformation, *Nature* **442**, 904 (2006).
  - [3] A. Aviram and M. A. Ratner, Molecular rectifiers. *Chem. Phys. Lett.* **29**, 277 (1974).
  - [4] K. Joulain, J. Drevillon, Y. Ezzahri and J. Ordenez-Miranda, Quantum Thermal Transistor. *Phys. Rev. Lett.* **116**, 200601 (2016).
  - [5] J. Ren, P. Hänggi and B. Li, Berry-Phase-Induced Heat Pumping and Its Impact on the Fluctuation Theorem. *Phys. Rev. Lett.* **104**, 170601 (2010).
  - [6] N. A. Sinitsyn and I. Nemenman, The Berry phase and the pump flux in stochastic chemical kinetics. *EPL*, **77**, 58001 (2007).
  - [7] I. Franco, M. Shapiro and P. Brumer, Robust ultrafast currents in molecular wires through stark shifts. *Phys. Rev. Lett.* **99**, 126802 (2007).
  - [8] A. Gambetta, C. Manzoni, E. Menna, M. Meneghetti, G. Cerullo, G. Lanzani, S. Tretiak, A. Piryatinski, A. Saxena, R. L. Martin and A. R. Bishop. Real-time observation of nonlinear coherent phonon dynamics in single-walled carbon nanotubes. *Nat. Phys.* **2**, 515 (2006).
  - [9] S. Tretiak, A. Saxena, R. L. Martin and A. R. Bishop, Conformational dynamics of photoexcited conjugated molecules. *Phys. Rev. Lett.* **89**, 097402 (2002).
  - [10] F. Santandrea, L. Y. Gorelik, R. I. Shekhter and M. Jonsson. Cooling of Nanomechanical Resonators by Thermally Activated Single-Electron Transport. *Phys. Rev. Lett.* **106**, 186803 (2011).
  - [11] S. Zippilli, G. Morigi, and A. Bachtold. Cooling Carbon Nanotubes to the Phononic Ground State with a Constant Electron Current. *Phys. Rev. Lett.* **102**, 096804 (2009).
  - [12] R. Härtle and M. Thoss, Resonant electron transport in single-molecule junctions: Vibrational excitation, rectification, negative differential resistance, and local cooling. *Phys. Rev. B* **83**, 115414 (2011).
  - [13] S. Walter, B. Trauzettel and Thomas L. Schmidt, Transport properties of double quantum dots with electron-phonon coupling. *Phys. Rev. B* **88**, 195425 (2013).
  - [14] A. Zazunov, D. Feinberg, and T. Martin. Phonon-mediated negative differential conductance in molecular quantum dots. *Phys. Rev. B* **73**, 115405 (2006).
  - [15] D. Boese and H. Schoeller, Influence of nanomechanical properties on single-electron tunneling: A vibrating single-electron transistor. *EPL* **54**, 668 (2001).
  - [16] Z.-Z. Chen, R. Lü and B.-F. Zhu, Effects of electron-phonon interaction on nonequilibrium transport through a single-molecule transistor, *Phys. Rev. B* **71**, 165324 (2005).
  - [17] R. Egger and A. O. Gogolin, Vibration-induced correction to the current through a single molecule. *Phys. Rev. B* **77**, 113405 (2008).
  - [18] J. Koch, M. Semmelhack, F. von Oppen, and A. Nitzan, Current-induced nonequilibrium vibrations in single-molecule devices. *Phys. Rev. B* **73**, 155306 (2006).
  - [19] J. Paaske and K. Flensberg, Vibrational Sidebands and the Kondo Effect in Molecular Transistors. *Phys. Rev. Lett.* **94**, 176801 (2005).
  - [20] A. Yar, A. Donarini, S. Koller and M. Grifoni, Dynamical symmetry breaking in vibration-assisted transport through nanostructures. *Phys. Rev. B* **84**, 115432 (2011).
  - [21] M. Galperin, M. A. Ratner and A. Nitzan, Molecular transport junctions: vibrational effects. *J. Phys. Condens. Matter* **19**, 103201 (2007).
  - [22] Y. Kim, H. Song, F. Strigl, H.-F. Pernau, T. Lee, and E. Scheer, Conductance and vibrational states of single-molecule junctions controlled by mechanical stretching and material variation. *Phys. Rev. Lett.* **106**, 196804 (2011).
  - [23] M. L. Perrin, C. J. O. Verzijl, C. A. Martin, A. J. Shaikh, R. Eelkema, J. H. Van Esch, J. M. van Ruitenbeek, J. M. Thijssen, H. S. J. van der Zant, D. Dulić, Large tunable image-charge effects in single-molecule junctions. *Nat. Nanotechnol.* **8**, 282 (2013).
  - [24] S. A. Gurvitz and Ya. S. Prager, Microscopic derivation of rate equations for quantum transport. *Phys. Rev. B* **53**, 15932 (1996).
  - [25] U. Harbola, M. Esposito and S. Mukamel, Quantum master equation for electron transport through quantum dots and single molecules. *Phys. Rev. B* **74**, 235309 (2006).
  - [26] J. P. Garrahan and I. Lesanovsky. Thermodynamics of quantum jump trajectories. *Phys. Rev. Lett.* **104**, 160601 (2010).
  - [27] S. Pigeon, L. Fusco, A. Xuereb, G. De Chiara and M. Paternostro, Thermodynamics of trajectories of a quantum harmonic oscillator coupled to  $N$  baths. *Phys. Rev. A* **92**, 013844 (2015).
  - [28] S. Pigeon and A. Xuereb, Thermodynamics of trajectories of open quantum systems, step by step. *J. Stat. Mech.*, 063203 (2016).
  - [29] N. Lambert, Y.-N. Chen, Y.-C. Cheng, C.-M. Li, G.-Y. Chen and F. Nori, Quantum biology. *Nat. Phys.* **8**, 10 (2012).
  - [30] F. Levi, S. Mostarda, F. Rao and F. Mintert. Quantum mechanics of excitation transport in photosynthetic complexes: a key issues review. *Rep. Prog. Phys.* **78**, 082001 (2015).
  - [31] R. De J. Leòn-Montiel and J. P. Torres, Highly efficient noise-assisted energy transport in classical oscillator systems. *Phys. Rev. Lett.* **110**, 218101 (2013).
  - [32] M. B. Plenio and S. F. Huelga, Dephasing-assisted transport: Quantum networks and biomolecules. *New J. Phys.* **10**, 113019 (2008).
  - [33] S. Viciani, M. Lima, M. Bellini and F. Caruso, Observation of Noise-Assisted Transport in an All-Optical Cavity-Based Network. *Phys. Rev. Lett.* **115**, 083601 (2015).

- [34] L. Gammaitoni, P. Hänggi, P. Jung and F. Marchesoni, Stochastic resonance. *Rev. Mod. Phys.* **70**, 223 (1998).  
 [35] C. Bushdid, M. O. Magnasco, L. B. Vosshall and A. Keller, Humans can discriminate more than 1 trillion olfactory stimuli. *Science* **343**, 1370 (2014).  
 [36] L. Turin, A Method for the Calculation of Odor Character from Molecular Structure. *J. Theor. Biol.*, **216** 367 (2002).  
 [37] J. C. Brookes, F. Hartoutsiou, A. P. Horsfield and A. M. Stoneham. Could humans recognize odor by phonon as-

sisted tunneling? *Phys. Rev. Lett.*, **98** 038101 (2007).

### Appendix 1: Dissipation of the wire to the leads and biased contribution to the evolution

In this appendix we detail the calculation leading to the Lindblad form dissipator induced by coupling the wire subsystem to fermionic leads as explained in section IB. Based on Refs. [24, 25] we determine the the dissipator in the manybody picture such as  $\tilde{\mathcal{L}}^\nu = \sum_{a=1}^2 \sum_{b=\{0,3\}} \tilde{\mathcal{L}}_{a \leftrightarrow b}^\nu$  (with  $\nu = R$  or  $L$ )

$$\begin{aligned} \tilde{\mathcal{L}}_{a \leftrightarrow 0}^\nu[\bullet] &= \frac{\pi}{4} \Gamma^\nu n_\nu(\epsilon_a) |T_{2,a}^\nu|^2 \left[ f_\nu(\epsilon_a) (2\hat{c}_a^\dagger \bullet \hat{c}_a - \{\hat{c}_a \hat{c}_a^\dagger, \bullet\}) + (1 - f_\nu(\epsilon_a)) (2\hat{c}_a \bullet \hat{c}_a^\dagger - \{\hat{c}_a^\dagger \hat{c}_a, \bullet\}) \right] \\ \tilde{\mathcal{L}}_{a \leftrightarrow 3}^\nu[\bullet] &= \frac{\pi}{4} \Gamma^\nu n_\nu(\epsilon_a) |T_{1,a}^\nu|^2 \left[ f_\nu(\epsilon_a) (2\hat{c}_3^\dagger \hat{c}_3 \bullet \hat{c}_a^\dagger \hat{c}_a - \{\hat{c}_3^\dagger \hat{c}_a \hat{c}_3^\dagger \hat{c}_3, \bullet\}) + (1 - f_\nu(\epsilon_a)) (2\hat{c}_3^\dagger \hat{c}_a \bullet \hat{c}_a^\dagger \hat{c}_3 - \{\hat{c}_a^\dagger \hat{c}_3 \hat{c}_3^\dagger \hat{c}_a, \bullet\}) \right] \end{aligned} \quad (29)$$

where  $n_\nu(\epsilon)$  is the density of state in the lead  $\nu$  ( $R$  or  $L$ ) at a given energy and  $f_\nu(\epsilon) = 1 / [\exp((\epsilon - \mu_\nu) / k_B T_\nu) + 1]$  the Fermi distribution of a given lead  $\nu$  having  $\mu_\nu$  as chemical potential. Notice that the total dissipation is related to the leads dissipation  $\tilde{\mathcal{L}} = \tilde{\mathcal{L}}^R + \tilde{\mathcal{L}}^L$  plus  $\tilde{\mathcal{L}}_{\text{eff}} = U^{-1} \mathcal{L}_{\text{eff}} U$  the one induced by the vibrational mode (Eq. (13)). Each dissipation induced by the leads can be decomposed in terms of amplitude damping and coherence damping channels such as  $\mathcal{L} = \mathcal{L}_A + \mathcal{L}_C$ , with for the amplitude part

$$\mathcal{L}_A[\bullet] = \sum_{XY=\{LO, LF, RO, RF\}} \left[ \alpha_{XY} \left( \hat{L}_{XY} \bullet \hat{L}_{XY}^\dagger - \frac{1}{2} \{ \hat{L}_{XY}^\dagger \hat{L}_{XY}, \bullet \} \right) + \beta_{XY} \left( \hat{L}_{XY}^\dagger \bullet \hat{L}_{XY} - \frac{1}{2} \{ \hat{L}_{XY} \hat{L}_{XY}^\dagger, \bullet \} \right) \right], \quad (31)$$

with  $\hat{L}_{LO} = |10\rangle\langle 00|$ ,  $\hat{L}_{LF} = |10\rangle\langle 11|$ ,  $\hat{L}_{RO} = |01\rangle\langle 00|$  and  $\hat{L}_{RF} = |01\rangle\langle 11|$  and for the coupling strength we have

$$\alpha_{LO} = \frac{\Gamma}{2} \left[ (1 - A)^2 (f_L(\epsilon_1) B^2 + f_R(\epsilon_1) (1 - A)^2) + (1 + A)^2 [f_L(\epsilon_2) B^2 + f_R(\epsilon_2) (1 + A)^2] \right] \quad (32)$$

$$\alpha_{LF} = \frac{\Gamma}{2} \left[ (1 - A)^2 (f_L(\epsilon_1) (1 - A)^2 + f_R(\epsilon_1) B^2) + (1 + A)^2 (f_L(\epsilon_2) (1 + A)^2 + f_R(\epsilon_2) B^2) \right] \quad (33)$$

$$\alpha_{RO} = \frac{\Gamma}{2} \left[ B^2 (f_L(\epsilon_1) + f_L(\epsilon_2)) + (f_R(\epsilon_1) (1 - A)^2 + f_R(\epsilon_2) (1 + A)^2) \right] \quad (34)$$

$$\alpha_{RF} = \frac{\Gamma}{2} \left[ (f_L(\epsilon_1) (1 - A)^2 + f_L(\epsilon_2) (1 + A)^2) + B^2 (f_R(\epsilon_1) + f_R(\epsilon_2)) \right]. \quad (35)$$

For simplicity we assume the leads density of states to be homogenous and identical  $n_L(\epsilon) = n_R(\epsilon) = n$  as for the coupling strength  $\Gamma^L = \Gamma^R = \Gamma / n\pi$ . The coefficients  $\beta_{XY}$  are obtained replacing in the definition above  $f_\nu(\epsilon) \rightarrow 1 - f_\nu(\epsilon)$ . The effective decoherence is written as

$$\mathcal{L}_C[\bullet] = \sum_{\substack{XY=\{LO, LF, RO, RF\} \\ AB=\{RO, RF, LO, LF\}}} \left[ \alpha_{XY}^c \left( \hat{L}_{XY} \bullet \hat{L}_{AB}^\dagger - \frac{1}{2} \{ \hat{L}_{AB}^\dagger \hat{L}_{XY}, \bullet \} \right) + \beta_{XY}^c \left( \hat{L}_{AB}^\dagger \bullet \hat{L}_{XY} - \frac{1}{2} \{ \hat{L}_{XY} \hat{L}_{AB}^\dagger, \bullet \} \right) \right]. \quad (36)$$

It is worth to notice that those dissipator acting on the coherence are not of a dephasing form because they change the energy of the system. They give rise to or suppress coherences between the 2 intermediate states through absorption or emission of quanta of energy with the leads. The coupling strength attached to those channels are such as

$$\alpha_O^c = \alpha_{LO}^c = \alpha_{RO}^c = \frac{\Gamma}{2} \left[ (1 - A) (f_L(\epsilon_1) B^2 + f_R(\epsilon_1) (1 - A)^2) - (1 + A) (f_L(\epsilon_2) B^2 + f_R(\epsilon_2) (1 + A)^2) \right] \quad (37)$$

$$\alpha_F^c = \alpha_{LF}^c = \alpha_{RF}^c = \frac{\Gamma}{2} \left[ (1 - A) (f_L(\epsilon_1) (1 - A)^2 + f_R(\epsilon_1) B^2) - (1 + A) (f_L(\epsilon_2) (1 + A)^2 + f_R(\epsilon_2) B^2) \right]. \quad (38)$$

In order to retrieve the exchange statistics we define as done in the text (section II A) a counting process  $K$  which is related to a biased contribution of the evolution  $\mathcal{L}_s$  where

$$\begin{aligned} \mathcal{L}_s[\bullet] = & \sum_{b=\{O,F\}} \sum_{a=\{L,R\}} \left[ \left( e^{(-1)^b s} - 1 \right) \left( \alpha_b^{Rc} |a\rangle \langle b| \bullet |b\rangle \langle \bar{a}| + \alpha_{ab}^R |10\rangle \langle b| \bullet |b\rangle \langle 10| \right) \right. \\ & \left. + \left( e^{(-1)^{b+1} s} - 1 \right) \left( \beta_b^{Rc} |b\rangle \langle a| \bullet |\bar{a}\rangle \langle b| + \beta_{ab}^R |b\rangle \langle a| \bullet |a\rangle \langle b| \right) \right] \end{aligned} \quad (39)$$

with  $\bar{a}$  is the complementary of  $a$  ( $R$  for  $L$  and reciprocally).

## Appendix 2: Superoperator of the effective electronic dynamics

Here we provide the explicit form of the superoperator responsible for the effective open-system dynamics of the electronic system discussed in Sec. II. With the definitions of the previous Appendix, we have

$$\mathcal{W} = \begin{pmatrix} -(\alpha_{0,0} + \alpha_{0,2}) & \beta_{RO} & \beta_{LO} & 0 & \beta_O^c & \beta_O^c \\ \alpha_{RO} & -(\beta_{RF} + \beta_{RO}) - \Gamma_v & \Gamma_v & \alpha_{RF} & -\frac{1}{2}(\beta_O^c + \beta_F^c) & -\frac{1}{2}(\beta_O^c + \beta_F^c) \\ \alpha_{LO} & \Gamma_v & -(\beta_{LO} + \beta_{LF}) - \Gamma_v & \alpha_{LF} & -\frac{1}{2}(\beta_O^c + \beta_F^c) & -\frac{1}{2}(\beta_O^c + \beta_F^c) \\ 0 & \beta_{RF} & \beta_{LF} & -(\alpha_{3,0} + \alpha_{3,2}) & \beta_F^c & \beta_F^c \\ \alpha_O^c & -\frac{1}{2}(\beta_O^c + \beta_F^c) & -\frac{1}{2}(\beta_O^c + \beta_F^c) & \alpha_F^c & -i\Delta - \Gamma_v - \frac{1}{2}\beta & \Gamma_v \\ \alpha_O^c & -\frac{1}{2}(\beta_O^c + \beta_F^c) & -\frac{1}{2}(\beta_O^c + \beta_F^c) & \alpha_F^c & \Gamma_v & i\Delta - \Gamma_v - \frac{1}{2}\beta \end{pmatrix} \quad (40)$$

with  $\beta = \beta_{LO} + \beta_{LF} + \beta_{RF} + \beta_{RO}$  and  $\Delta = \epsilon_R - \epsilon_L$ . The explicit definition of each coefficient is given in Appendix IV. Notice that each coefficient  $\alpha$  and  $\beta$  can be easily rewritten in terms of leads contribution such as  $\alpha_{XY} = \alpha_{XY}^R + \alpha_{XY}^L$ .

The effective dissipator of the biased master equation resulting from the inclusion of counting processes has the following matrix representation, instead

$$\mathcal{L}_s = \begin{pmatrix} 0 & \beta_{RO}^R (e^{-s} - 1) & \beta_{LO}^R (e^{-s} - 1) & 0 & \beta_O^{Rc} (e^{-s} - 1) & \beta_O^{Rc} (e^{-s} - 1) \\ \alpha_{RO}^R (e^s - 1) & 0 & 0 & \alpha_{RF}^R (e^{-s} - 1) & 0 & 0 \\ \alpha_{LO}^R (e^s - 1) & 0 & 0 & \alpha_{LF}^R (e^{-s} - 1) & 0 & 0 \\ 0 & \beta_{RF}^R (e^s - 1) & \beta_{LF}^R (e^s - 1) & 0 & \beta_F^{Rc} (e^s - 1) & \beta_F^{Rc} (e^s - 1) \\ \alpha_O^{Rc} (e^s - 1) & 0 & 0 & \alpha_F^{Rc} (e^{-s} - 1) & 0 & 0 \\ \alpha_O^{Rc} (e^s - 1) & 0 & 0 & \alpha_F^{Rc} (e^{-s} - 1) & 0 & 0 \end{pmatrix}. \quad (41)$$